# Large Eddy / Reynolds-Averaged Navier-Stokes Simulations of CUBRC Base Heating Experiments

Giovanni Salazar and Jack R. Edwards
*North Carolina State University, Raleigh, NC, 27695*

and
Adam J. Amar
*NASA Lyndon B. Johnson Space Center, Houston, TX, 77058*

## I. Introduction

Even with great advances in computational techniques and computing power during recent decades, the modeling of unsteady separated flows, such as those encountered in the wake of a re-entry vehicle, continues to be one of the most challenging problems in CFD. Of most interest to the aerothermodynamics community is accurately predicting transient heating loads on the base of a blunt body, which would result in reduced uncertainties and safety margins when designing a re-entry vehicle. However, the prediction of heat transfer can vary widely depending on the turbulence model employed. Therefore, selecting a turbulence model which realistically captures as much of the flow physics as possible will result in improved results. Reynolds Averaged Navier Stokes (RANS) models have become increasingly popular due to their good performance with attached flows, and the relatively quick turn-around time to obtain results. However, RANS methods cannot accurately simulate unsteady separated wake flows, and running direct numerical simulation (DNS) on such complex flows is currently too computationally expensive. Large Eddy Simulation (LES) techniques allow for the computation of the large eddies, which contain most of the Reynolds stress, while modeling the smaller (subgrid) eddies. This results in models which are more computationally expensive than RANS methods, but not as prohibitive as DNS. By complimenting an LES approach with a RANS model, a hybrid LES/RANS method resolves the larger turbulent scales away from surfaces with LES, and switches to a RANS model inside boundary layers. As pointed out by Bertin et al., this type of hybrid approach has shown a lot of promise for predicting turbulent flows, "but work is needed to verify that these models work well in hypersonic flows[1]."

The very limited amounts of flight and experimental data available presents an additional challenge for researchers. Recently, a joint study by NASA and CUBRC has focused on collecting heat transfer data on the backshell of a scaled model of the Orion Multi-Purpose Crew Vehicle (MPCV). Heat augmentation effects due to the presence of cavities and RCS jet firings were also investigated. The high quality data produced by this effort presents a new set of data which can be used to assess the performance of CFD methods. In this work, a hybrid LES/RANS model developed at North Carolina State University (NCSU) is used to simulate several runs from these experiments, and evaluate the performance of high fidelity methods as compared to more typical RANS models.

.

## II. Experimental Details and Test Conditions

The experiments were carried out by CUBRC in the LENS 1 reflected shock tunnel in Buffalo, NY. A 10-inch diameter (5% scale) model of NASA's Orion MPCV was equipped with 290 heat transfer sensors and 10 pressure gauges. Most heat transfer gauges were thin-film sensors, and some coaxial thermocouples were also installed. The majority of sensors were placed on the backshell of the vehicle since this was the primary region of interest

during these experiments. The model also included two roll RCS jets, two pitch down RCS jets, and a launch abort system (LAS) cavity on the windward side of the model.

The tests were carried out at different Reynolds numbers, angles of attack, and freestream enthalpies for a Mach 8 nominal freestream. The Reynolds numbers tested spanned from $\mathrm{Re}_D = 2\times10^6$ to $\mathrm{Re}_D = 15\times10^6$ where $\mathrm{Re}_D$ is the Reynolds number based on capsule diameter (*D*). Currently, only one experimental run has been simulated in this work. We selected the highest Reynolds number condition, which represents an excellent test case for our hybrid LES/RANS method since this case presents the highest degrees of turbulence. Different test gases and combinations of RCS jets firing were also tested. However, due to the complexity of simulating the problem with RCS jets firing, the experimental run considered in this work did not include any jets firing. The experimental run conditions are summarized in Table 1.

**Table 1.** *Testing conditions for Run5.*

| | **Run 5 (Turbulent Flow)** |
|---|---|
| Test Gas | $N_2$ |
| AoA (deg) | 18 |
| $Re_D$ | $15.5\times10^6$ |
| $M_\infty$ | 8 |
| $\rho_\infty$ (kg/ $m^3$) | 0.2402 |
| $U_\infty$ (m/s) | 1517.9 |
| $T_{wall}$ (K) | 295.56 |
| $T_\infty$ (K) | 86.67 |

## III. Numerical method

The computations were performed using NCSU's in-house code REACTMB. This model solves the three-dimensional, unsteady compressible Navier-Stokes equations for a mixture of thermally perfect gases, using a thin layer formulation. It employs a finite volume discretization and is used for solving problems on multi-block structured meshes. A Crank-Nicholson type discretization with a planar relaxation subiteration procedure is used for time advancement. For parallel communication, REACTMB uses MPI message passing.

The specific heats and enthalpies are computed using thermodynamic curve fits obtained from McBride, et al.[2], the mixture thermal conductivity is obtained by assuming a constant Prandtl number of 0.72, the mixture viscosity is computed using Wilke's law, and molecular diffusion is taken into account by keeping a constant Schmidt number of 0.5. Additionally, when considering chemical reactions, the law of mass action is used to formulate the source terms. However, in the present work, no reactions where considered and the gas was assumed to be calorically perfect.

### A. Evaluation of fluxes

Viscous fluxes are computed using central differences. Inviscid fluxes are evaluated using Edwards' low-diffusion flux-splitting scheme (LDFSS), and extended to higher order by using a piecewise parabolic method (PPM). Using the present formulation, the left and right states at a cell interface are calculated as :

$$V_{L,i+1/2} = (1 - f_i^P)V_{L,i+1/2}^H + f_i^P V_i$$

$$V_{R,i+1/2} = (1 - f_{i+1}^P)V_{R,i+1/2}^H + f_{i+1}^P V_{i+1}$$

where $V=[p,u,v,w,T,k,\omega]^T$ represents the vector of primitive variables, $f_i^P$ is a pressure limiter and $V_{R/L+1/2}^H$ is a higher-order interpolant. The pressure limiter used is defined as

$$f_i^P = 1.25\left[\max\left(\frac{|\Delta^2 p|}{|\Delta^2 p|+\overline{p}},0.2\right)-0.2\right],\ \Delta^2 p = p_{i+1}-2p_i+p_{i-1},\ \overline{p}=\frac{1}{4}(p_{i+1}+2p_i+p_{i-1})$$

and it reduces the scheme's accuracy to first order in regions where the pressure field curvature is large. The higher-order interpolants are constructed by using an average cell value $V_{i+1/2}^c$, monotone interpolants $V_{L/R,i+1/2}^M$ obtained from the PPM scheme, and a blending function $f_{i+1/2}^D$:

$$V_{L,i+1/2}^H = V_{i+1/2}^c + f_{i+1/2}^D(V_{L,i+1/2}^M - V_{i+1/2}^c)$$
$$V_{R,i+1/2}^H = V_{i+1/2}^c + f_{i+1/2}^D(V_{R,i+1/2}^M - V_{i+1/2}^c)$$

The blending function is computed by using the aforementioned pressure limiter and the vorticity/divergence function of Ducros[3] such as:

$$f_{i+1/2}^D = \max\left(f_i^p, f_{i+1}^p, f_i^{Ducros}, f_{i+1}^{Ducros}\right)$$
$$f_i^{Ducros} = \frac{(\nabla\cdot\vec{V})_i^2}{(\nabla\cdot\vec{V})_i^2+|\nabla\times\vec{V}|_i^2+\varepsilon_i^2},\quad \varepsilon = 1\times10^{-8}V_\infty/\max(\overline{\Delta x},\overline{\Delta y},\overline{\Delta z})$$

By becoming active in regions of high vorticity, the Ducros blending function limits the dissipation introduced by the monotonic reconstruction scheme in regions where turbulence scales can be resolved. The averaging operator implemented yields a fourth-order central difference method on uniform meshes, and is defined as:

$$V_{i+1/2}^c = \frac{7}{12}(V_i+V_{i+1})-\frac{1}{12}(V_{i+2}-V_{i-1})$$

**B. Turbulence closure**

The LES/RANS model is based on Menter's baseline $k-\omega$ model. The hybridization is accomplished by using the Boussinesq eddy-viscosity approximation, and defining the eddy viscosity as

$$\mu_t = \rho\left[\Gamma\frac{k}{\omega}+(1-\Gamma)\nu_{t,sgs}\right]$$

where $\rho$, $k$, and $\omega$ are the density, turbulence kinetic energy and specific dissipation rate, respectively. In addition, $\nu_{t,sgs}$ is the subgrid eddy viscosity and $\Gamma$ is a blending function, which is continuous in both space and time, and is defined as

$$\Gamma = \frac{1}{2}\left(1-\tanh\left[15\left(\frac{1}{\lambda^2}-1\right)\right]\right)$$

The definition of the blending function is based on the value of $\lambda$, which is a ratio of outer to inner length scales:

$$\lambda = \frac{l_{out}\, g(l_{out})}{l_{inn}} \ , \qquad g(l_{out}) = \min\left[10, \max\left(1, \frac{1}{2}\frac{\Delta_{\max}}{l_{out}}\right)\right]$$

$$l_{out} = \sqrt{\frac{10\nu\bar{\omega} + \bar{k} + \bar{k}_R}{C_\mu^{\,1/2}\bar{\omega}\omega}} \ , \quad l_{inn} = \kappa d$$

where $\nu$ is the kinematic viscosity, $k_R$ is the resolved kinetic energy, $\kappa$ is the von Kármán constant, $d$ is the distance from the nearest wall, $C_\mu$ is 0.09, and values with a bar over them indicate ensemble averaged values. This definition of $\lambda$, which includes a grid correction function $g(l_{out})$ , has been shown to produce a better response of the hybrid model and more accurate wall heat flux predictions, particularly inside boundary layers where the grid might not be fine enough to resolve the larger scale turbulence structures[4]. This approach results in a blending function which depends only on flow properties and does not require problem specific calibration[5].

## IV. Grid Design

A 29 M cell structured grid, which was suitable for both RANS and LES/RANS simulations, was created for the Orion capsule and sting configuration (Fig 1). In order for the LES/RANS method to properly resolve turbulent structures, a great amount of effort was devoted to keeping the cells in the wake region as orthogonal as possible, and small enough to resolve the most energetic eddies in the recirculation region. Previous experience using a grid designed by Barnhardt et al. for a similar problem[4,6], and best practices for our hybrid LES/RANS methods, were used to design the best grid possible for this case. The grid's outer surface was initially shock fitted using NASA's DPLR code, and using the highest Reynolds number conditions in order to use the same grid for other test cases. The sting was extended about 3 capsule diameters downstream with 248 cells in the streamwise direction along the sting. On the capsule geometry, the grid contains 172 off body cells, 320 cells in the circumference direction, and 210 cells along the backshell in the streamwise direction. The mesh was refined near the walls to resolve outer boundary layer turbulence, and in the wake region where the average cell size is less than 0.5% of the capsule diameter. Finally, the first wall normal cell spacing is $5\text{x}10^{-6}$ m for all walls, which has been determined to be adequate from experience with our numerical methods.

## V. Results

Four different solutions were computed for comparison: a laminar solution, a RANS solution using Menter BSL, an LES/RANS method using the PPM reconstruction, and an LES/RANS method using the PPM reconstruction and applying the low dissipation function of Ducros. This last method is termed Low Dissipation PPM (LDPPM) in the present study. Unsteady results using the LES/RANS model were started from a converged RANS solution. In order to collect statistics, the solution was advanced for 5-6 flow times (based on diameter) to ensure that the data being extracted at the gauge locations was statistically invariant, and then statistics were taken for an additional 5-6 flow times.

A supersonic inflow boundary condition was applied to the entire shock-fitted surface, since the grid was designed so that the shock is contained within, and the outflow plane was modeled using an extrapolation boundary condition. Additionally, the wall was treated as an isothermal wall due to the short test time durations experienced in the shock-tunnel, which is on the order of milliseconds. Nitrogen test gas was treated as a calorically perfect gas since the freestream enthalpy was low enough that no vibrational excitation of molecules nor dissociation would occur.

### A. LES/RANS solutions, PPM vs LDPPM

In this section the results obtained using the two different variants of LES/RANS methods (PPM and LDPPM) in order to assess the effect of using the low dissipation scheme. Figures 2-5 present instantaneous contours of Mach number, temperature, turbulent kinetic energy and transverse velocity at the symmetry plane for the solutions obtained using these two different schemes. The Mach number contours highlight some of the main features of this flow: a strong thin shock ahead of the capsule's forebody, a recompression region along the free shear layer where the flow is realigned with the freestream, and an additional shock on the windside which turns the flow due to the presence of the sting. As flow travels along the heatshield towards the leeside, the flow separates at the shoulder and results in a laminar unsteady shear layer which separates a subsonic recirculating region from the outer supersonic flow. An additional smaller recirculation region is also present on the windside base of the capsule. The temperature contours in Figure 3 show temperatures of up to 1200 K near the stagnation region, and increased temperatures present in the separated wake ranging from 600 K to 700 K.

Results using both LES/RANS schemes appear almost identical when looking at Mach number and temperature, however, the LDPPM scheme is able to resolve some smaller scales, as evidenced by the production of turbulent kinetic energy (TKE) in Figure 4, and the transverse velocity components observed in Figure 5. As expected, the PPM method results in additional numerical dissipation of turbulent structures, particularly further down the trailing wake. However, it is not clear how big of an effect this could have on wall heat flux levels, which is addressed in more detail in the next section.

### B. Pressure and heat flux comparisons with experiment

By comparing the experimental data at discrete locations with our CFD predictions, a direct assessment of the different models can be made. The data is compared to experimental values by using a standard percent error definition:

$$q_w(\%\,error) = \frac{q_{w\_\exp} - q_{w\_CFD}}{q_{w\_\exp}}$$

where $q_w$ represents wall heat flux. However, the error definition was also used to calculate percent error for pressure data. Quantitative comparisons with experimental data are shown in Figures 6-8 by plotting the percent error at each gauge location on the surface of the model. It is important to note that even though the plots show the different cavities which were exposed during the experiments, the simulations in the present study are carried out on a smooth capsule geometry.

Figure 6 shows the wall pressure percent error on the backshell using a laminar model (6a), RANS (6b), LES/RANS PPM (6c) and LES/RANS LDPPM (6d). Only 9 out of the 10 gauges are shown because one of the gauges was off during this run. The figures are oriented in such a way the bottom of the figure is the windside of the capsule, and

most of the pressure gauges are located on the separated region of the backshell. This orientation is consistent for all subsequent figures of the capsule's backshell. The wall pressure results show that all models do an excellent job of predicting the mean pressure at these locations within 35 % of the experimental values. The laminar, PPM and LDPPM models slightly overpredict pressure levels at all locations, while the RANS model underpredicts pressure at about half of the gauges, but still very close to experimental values. These results are consistent with the findings of Barnhardt et al.[6], who showed that laminar and turbulent models produced excellent agreements with experimental pressure levels for several different hypersonic flows.

Percent differences in heat flux levels on the forebody of the capsule are compared in Figure 7. The bottom of the forebody plots correspond to the side of the capsule where the flow is attached. By inspecting the percent differences produced by the laminar result, it is evident that as the flow travels along the heatshield, the boundary layer begins to transition to turbulent before the leeside shoulder is reached. However, the large overpediction of heat flux levels in regions closest to the leeside shoulder by the turbulence models suggests that the flow might not have completely transitioned to turbulent. Accurate prediction of heat flux levels in the forebody have proved to be challenging in other similar studies[6].

In Figure 8, the percent error distribution of backshell wall heat flux is shown for the four different simulations. Along the windside centerline, the laminar result predicts the first two heat gauges with very good accuracy (within 12% of experiment) indicating that the boundary layer is laminar at these two locations. On the other hand, all the turbulent models overpredict these two gauges by over 200% since no transition model is implemented in this study, but are able to accurately capture (within ~30%) the next two gauges downstream where the boundary layer has transitioned to turbulent. Furthermore, the LES/RANS schemes show almost exactly the same heat flux levels as RANS along regions where the flow is attached, indicating that the RANS model becomes active inside these boundary layers as expected. An analogous trend is observed on the next "ray" of gauges closest to the windside centerline.

As expected for such a high Reynolds number, the laminar result underpredicts heat fluxes for a large portion of the separated region by up to 100%. The RANS model almost uniformly overpredicts all sensor locations by up to 200% in some cases in the separated region. Because the laminar and RANS models bound the heat flux predictions at most locations, it is expected that a high fidelity model such as LES/RANS, would be able to capture the separated region with better accuracy. This is confirmed by looking at the PPM and LDPPM results in Figure 8, where more gauges are predicted within +/- 40% of the experiment in the separated region. Both LES/RANS schemes yield very similar results, and they both tend to underpredict experimental heat flux level by approximately 60-80% in regions closer to the leeside centerline. Some of the discrepancies between the LES/RANS results and the experiment in the separated region are due to the presence of the LAS well and RCS jet cavities present in the model during the experiment, while the simulations were carried out on a smooth body grid with no cavities.

A direct comparison between RANS, LES/RANS PPM, and LES/RANS LDPPM wall pressure distribution is shown in Figure 9. As expected, the different turbulence models predict different size and shape of the separation region, and these in turn have a direct impact on the surface heat flux and pressure distributions. The surface pressures shown for the unsteady LES/RANS methods are time averaged contours over 5-6 characteristic flow times based on the capsule diameter. The RANS model predicts a much smaller separation region, higher pressure gradients at the surface, and lower pressure values than LES/RANS. Because of the ability of the LES/RANS simulations to resolve a large range of turbulent scales in the separated region, mixing of the fluid within the separation region is enhanced and it leads to a more uniform wall pressure on the backshell. However, no significant differences are observed in the size and structure of the separation region, nor in the surface pressure distribution, between the PPM and the LDPPM schemes.

## VI. Upcoming Efforts

The results presented in this work so far, highlight the ability of LES/RANS methods to obtain more accurate aerothermodynamic environments than those obtained by using a more typical RANS model for hypersonic base flows. In addition, for this high Reynolds number case, the LDPPM scheme is able to resolve smaller turbulent scales throughout the wake, but no real gains were achieved in predicting wall heat flux levels as compared with the PPM scheme. The data presented in this study, and the CFD results, are very recent. Therefore additional analysis of the data and comparisons to CFD are currently being carried out to further evaluate the performance of these numerical methods for hypersonic base flows. In addition, other test cases at different Reynolds numbers are also being simulated using our hybrid LES/RANS schemes at this time.

## References


[1]Bertin, J.J., and Cummings, R.M. "Critical Hypersonic Aerothermodynamic Phenomena," Annu. Rev. Fluid Mech. 38, 2006, pp. 129-157.

[2]McBride, B.J., Gordon, S., and Reno, M.A. "Coefficients for Calculating Thermodynamic and Transport Properties of Individual Species," NASA TM-4513, 1993.

[3]Ducros, F., Ferrand, V., Nicaud, F., Weber, C., Darracq, D., Gachareiu, C., Poinsot, T. "Large-Eddy Simulation of the Shock / Turbulence Interaction," *Journal of Computational Physics*, Vol. 152, No. 2, 1999, pp. 517-549.

[4]Salazar, G., and Edwards, J.R. "Numerical Simulation of CUBRC Wake Flow Experiments Using a Hybrid LES/RANS Approach," AIAA Paper 2013-xxxx, 2013.

[5] Gieseking, D. A., Choi, J., Edwards, J. R., and Hassan, H. A., "Compressible-Flow Simulations Using a New Large-Eddy Simulation/Reynolds Averaged Navier-Stokes Model," AIAA Journal, Vol. 49, No. 10, 2011, pp. 2194-2209.

[6]Barnhardt, M., and Candler, G. V., "CFD Analysis of CUBRC Base Flow Experiments," AIAA Paper 2010-1250, 2010.

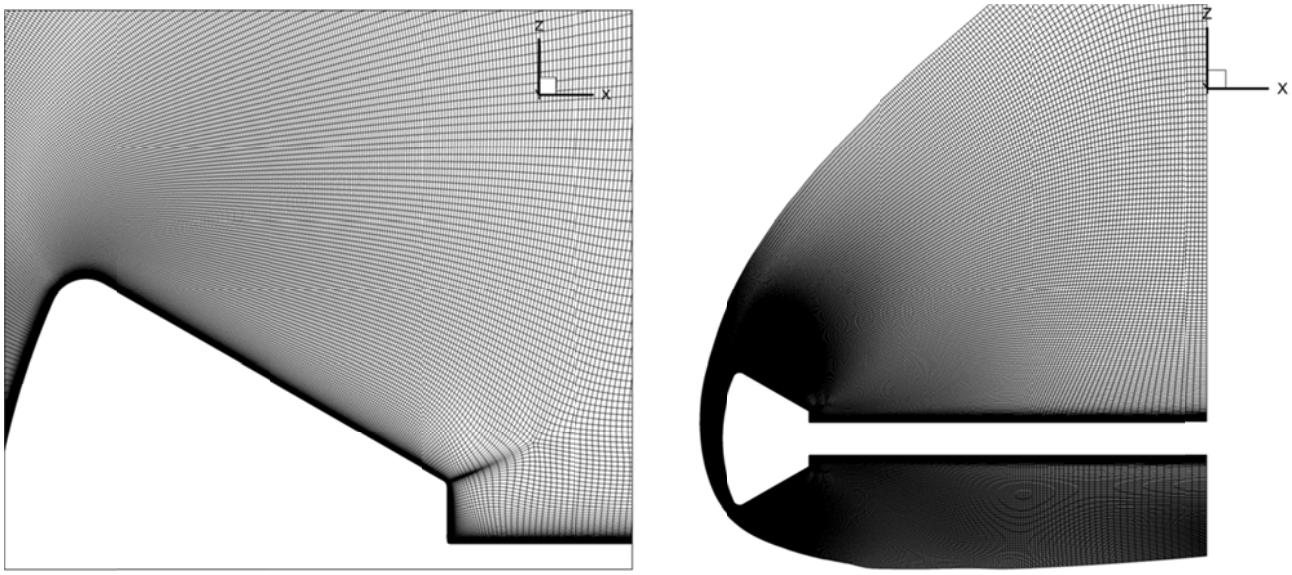


**Figure 1.** *Distribution of mesh cells in the symmetry plane of the domain (right), and detail view of mesh in the near wake region (left).*

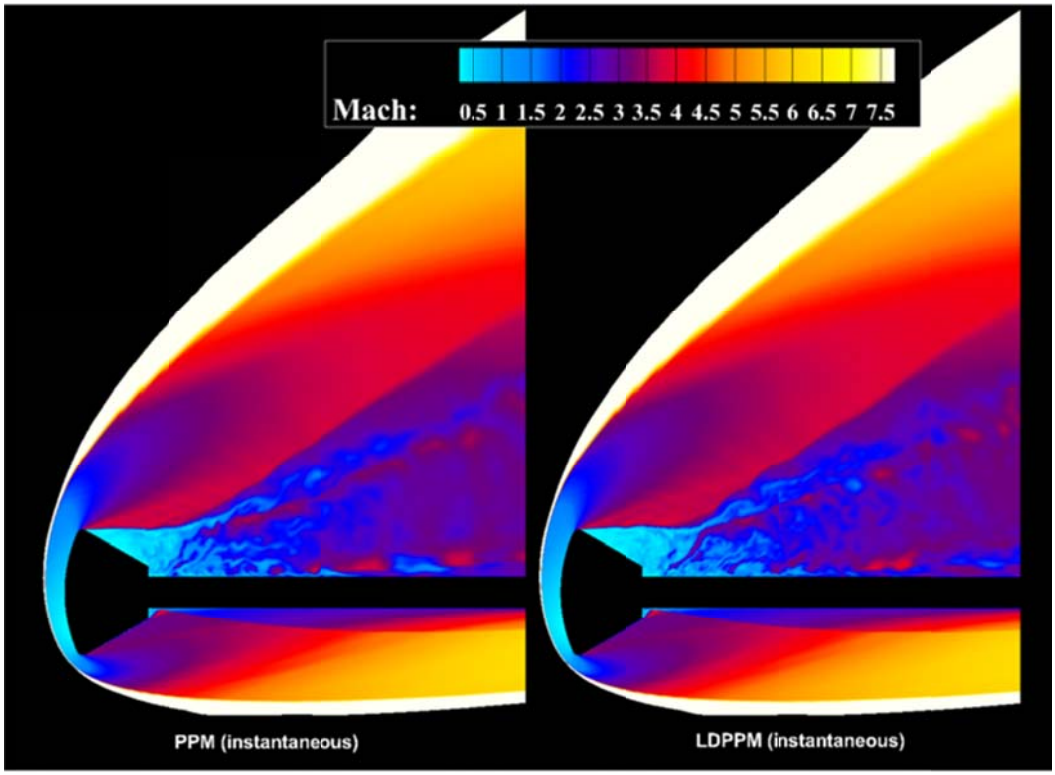


**Figure 2**. *Instantaneous Mach number contours obtained using PPM (left) and LDPPM (right) schemes.*

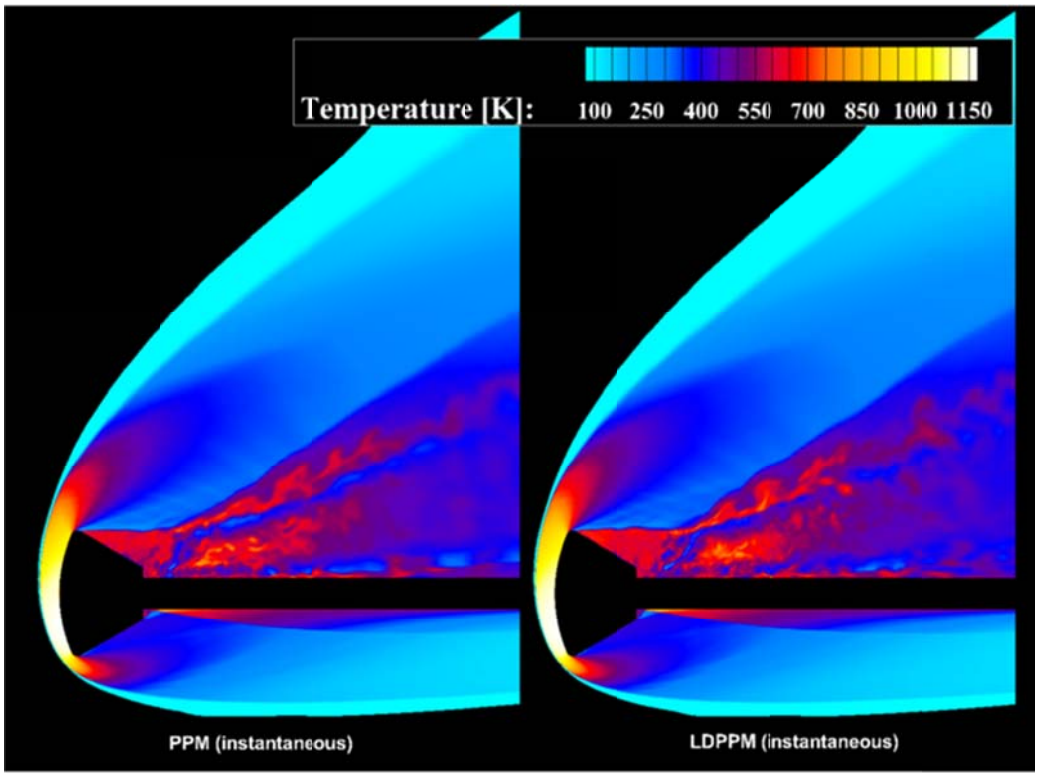


**Figure 3**. *Instantaneous temperature contours obtained using PPM (left) and LDPPM (right) schemes.*

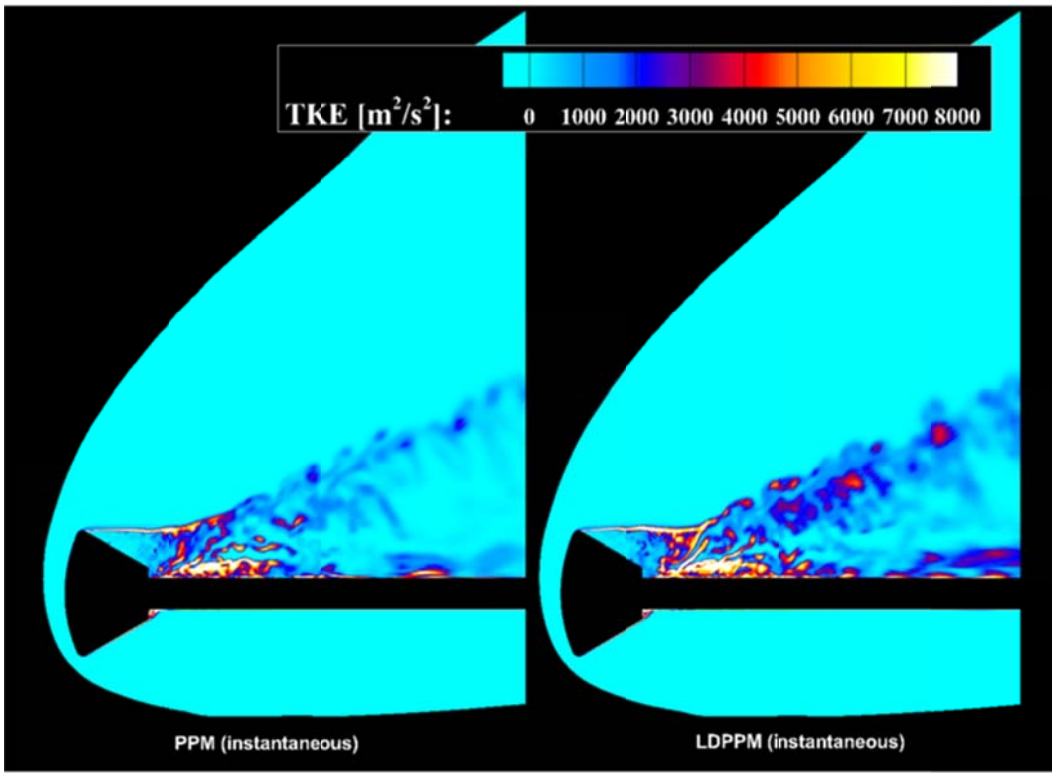


**Figure 4**. *Instantaneous turbulent kinetic energy contours obtained using PPM (left) and LDPPM (right) schemes.*

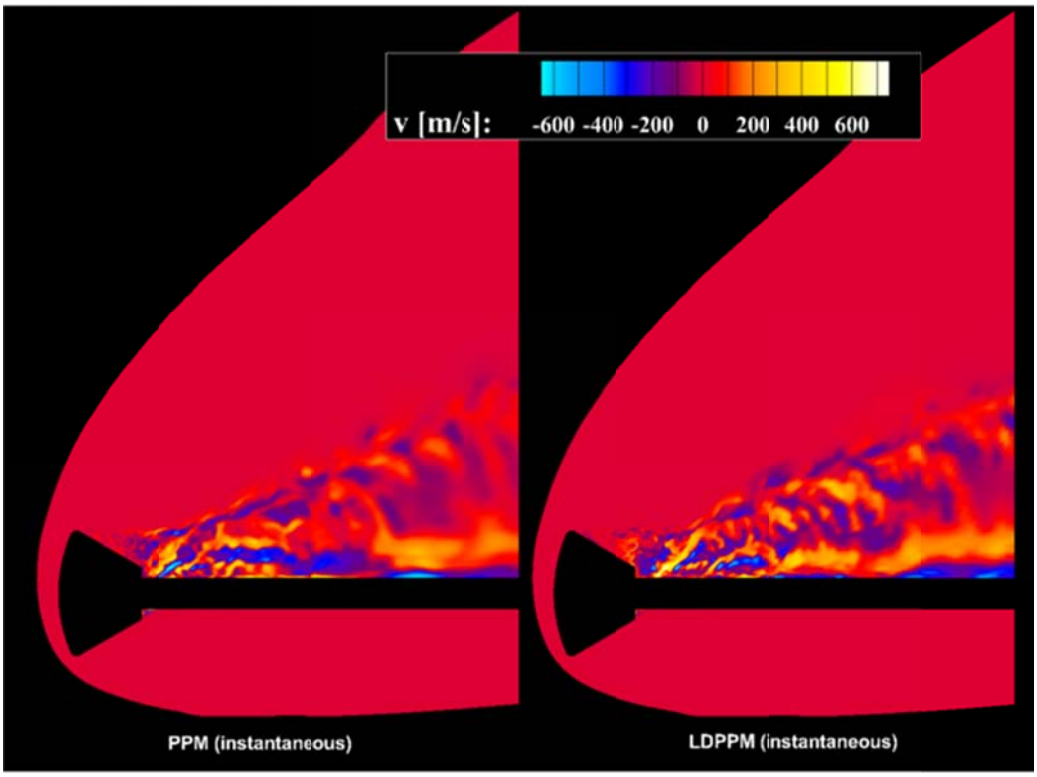


**Figure 5**. *Instantaneous transverse velocity contours obtained using PPM (left) and LDPPM (right) schemes.*

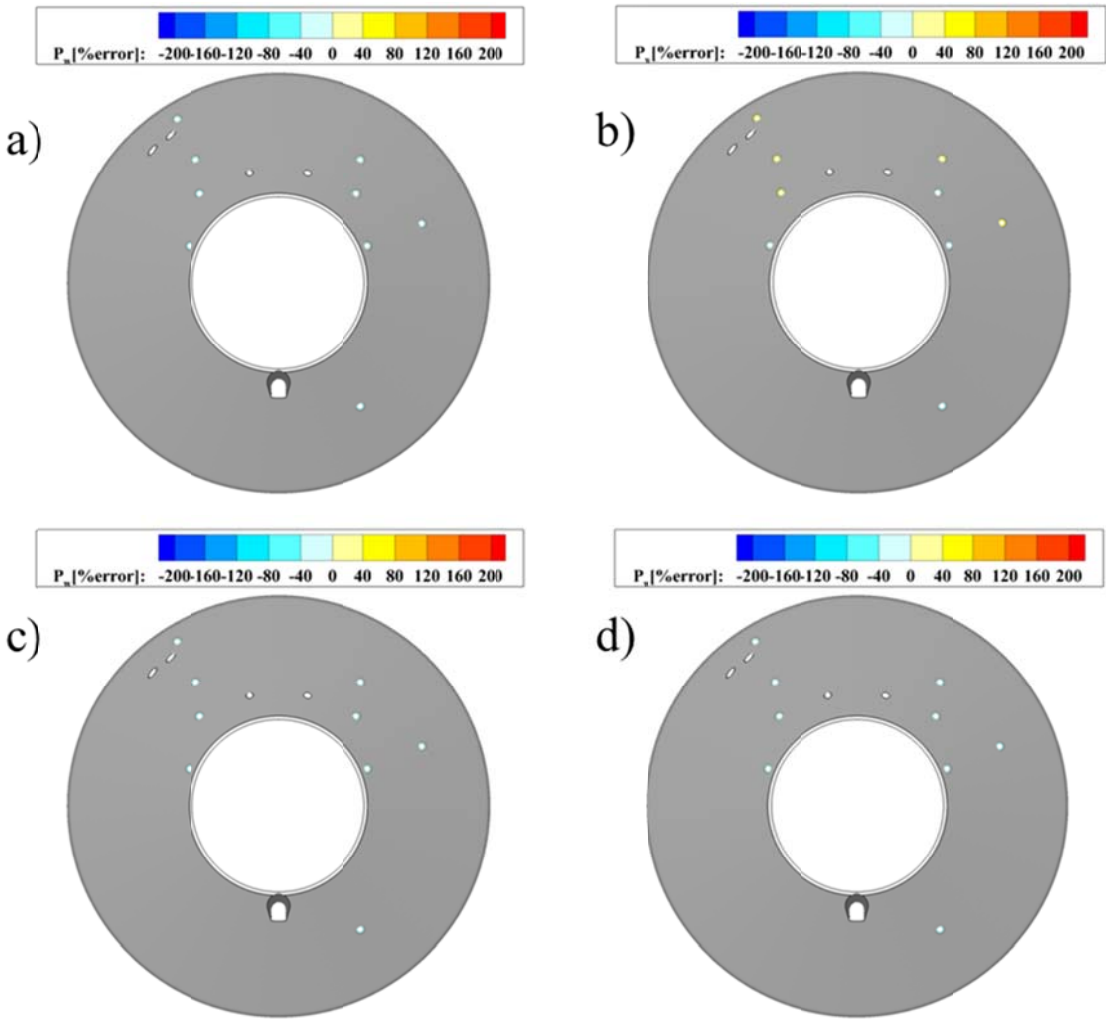


**Figure 6**. *Percent error at backshell pressure gauges obtained using a) laminar, b) RANS, c) LES/RANS PPM, and d) LES/RANS LDPPM methods.*

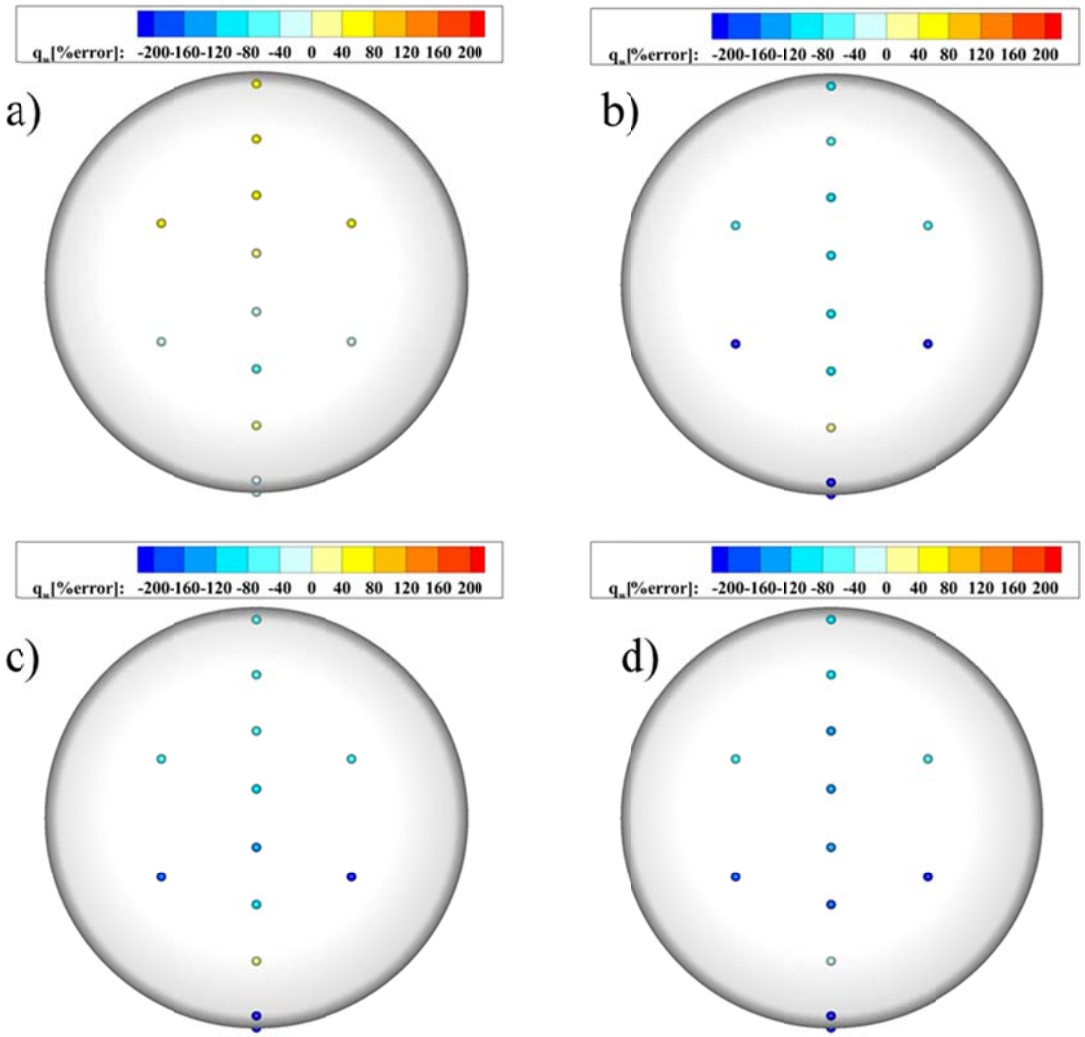


**Figure 7**. *Percent error at heatshield heat transfer gauges obtained using a) laminar, b) RANS, c) LES/RANS PPM, and d) LES/RANS LDPPM methods.*

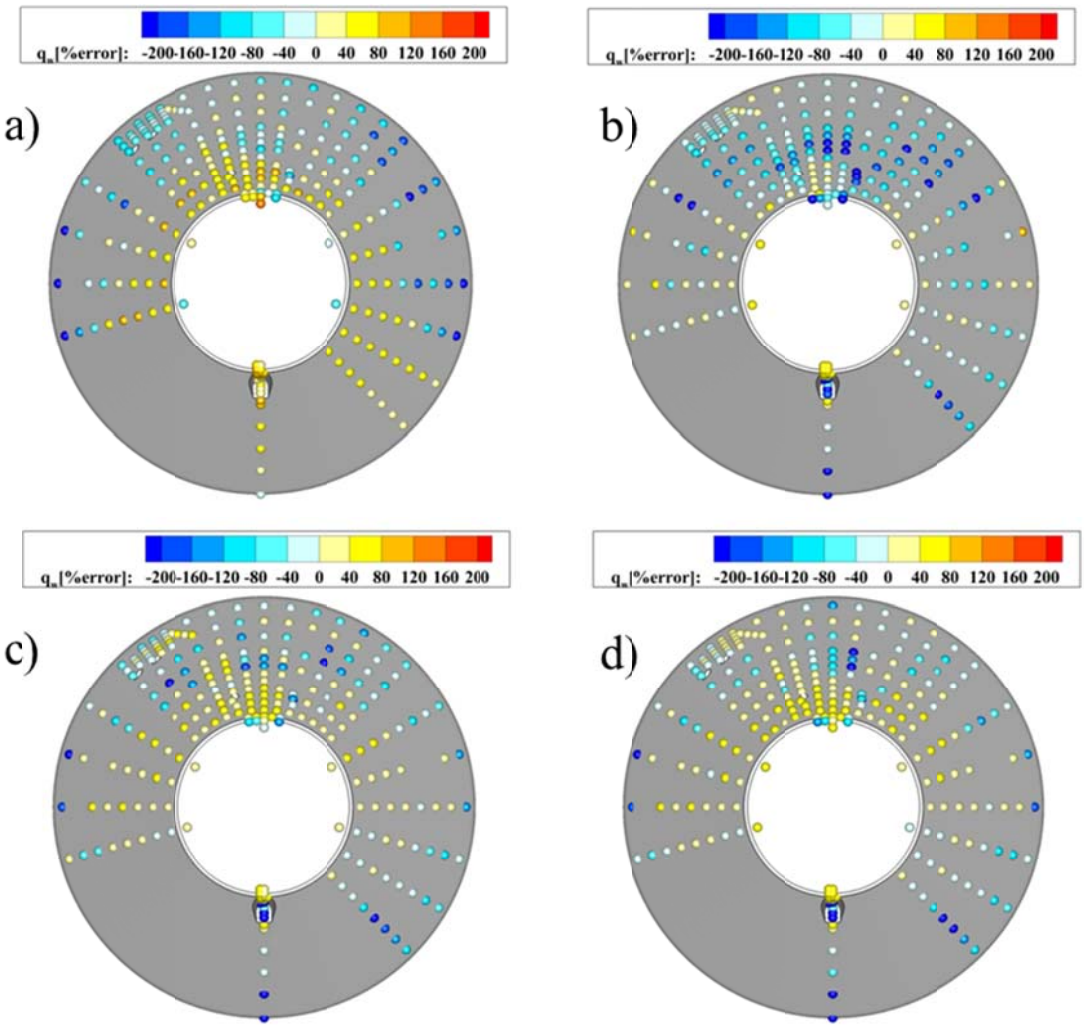


**Figure 8**. *Percent error at heatshield heat transfer gauges obtained using a) laminar, b) RANS, c) LES/RANS PPM, and d) LES/RANS LDPPM methods.*

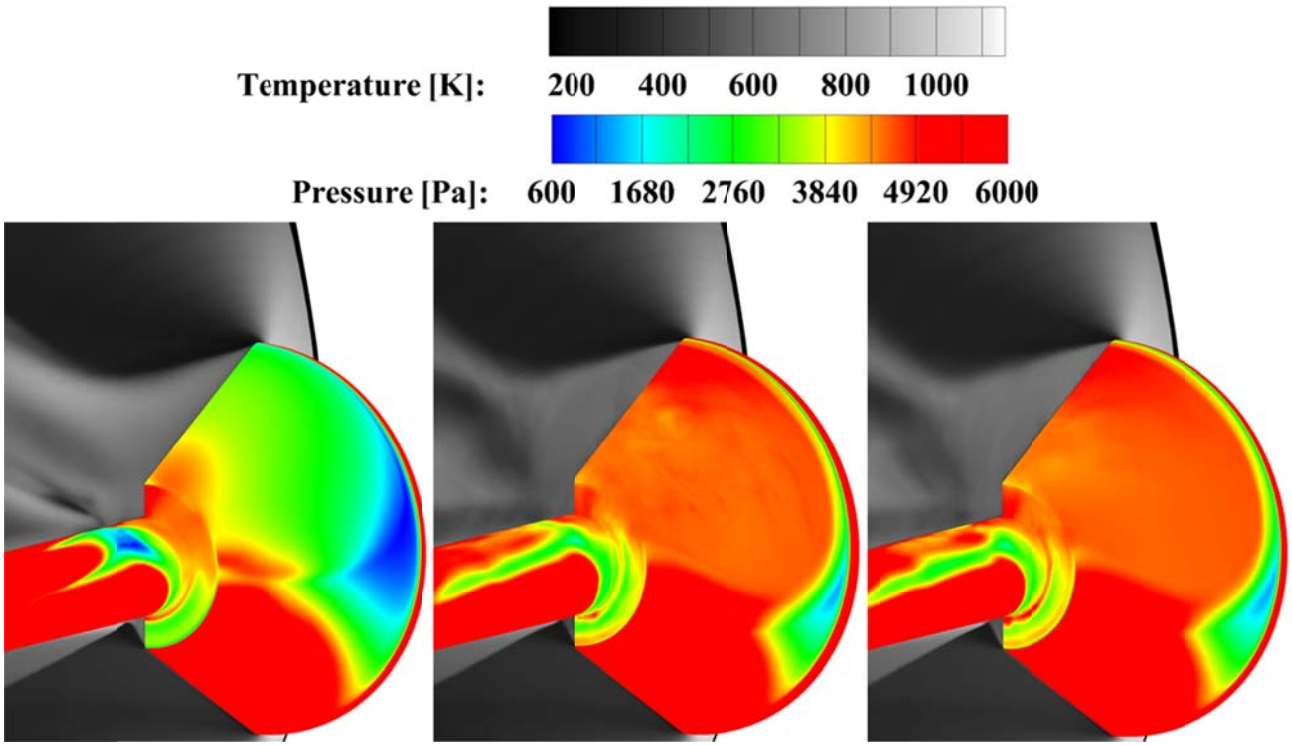


**Figure 9**. *Wall pressure contours with temperature contours on symmetry slice obtained using RANS (left), LES/RANS PPM (center), and LES/RANS LDPPM (right) models.*